Production and characterization of thin films based on soy protein isolate with kraft lignin and tannins obtained by casting

Anderson Júnior de Freitas[1], Nathielle Lourrane Vieira dos Santos Souza[3], Karoline Ferreira e Silva[1], Victor Wallace Ribeiro dos Santos[4], Isabela de Lourdes Valente[2], Marali Vilela Dias[5], José Manoel Marconcini[7], Fábio Akira Mori[6]

[1] Federal University of Lavras, School of Agricultural Sciences of Lavras, Graduate Program in Biomaterials Engineering, Lavras, Minas Gerais, Brazil.

[2] Federal University of Santa Maria, Department of Chemical Engineering, Graduate Program in Chemical Engineering, Santa Maria, Rio Grande do Sul, Brazil.

[3] Federal University of Lavras, Engineering School, Graduating in Chemical Engineering, Lavras, Minas Gerais, Brazil.

[4] Federal University of Lavras, Engineering School, Graduating in Mechanical Engineering, Lavras, Minas Gerais, Brazil.

[5] Federal University of Lavras, School of Agricultural Sciences of Lavras, Department of Food Sciences, Lavras, Minas Gerais, Brazil.

[6] Federal University of Lavras, School of Agricultural Sciences of Lavras, Departament of Forest Sciences, Lavras, Minas Gerais, Brazil.

[7] Embrapa Instrumentation, National Laboratory of Nanotechnology for Agribusiness, São Carlos, São Paulo, Brazil.

Correspondence: Anderson Júnior de Freitas, Federal University of Lavras, School of Agricultural Sciences of Lavras, Graduate Program in Biomaterials Engineering, Lavras, Minas Gerais, Brazil. E-mail: freitas.anderson01@gmail.com

Abstract

In the present study, soy protein isolate (SPI) multifunctional bioplastics were prepared by casting, with the addition of tannins extracted from *Stryphnodendron adstringens* and kraft lignin. The films were obtained through biopolymer composites and blends method, prepared at three pHs (8.5, 9.5 and 10.5) and characterized by thermochemical studies, Fourier-transform infrared spectroscopy, scanning electron microscopy, water vapor permeability (WVP), antioxidant activity, water contact angle, surface energy, wettability, and mechanical tests. The composites presented better results when compared to the blend and control films, respectively, in the polarity, hydrophobicity, WVP and especially in the antioxidant activity tests. Nevertheless, no significant difference between the samples was noticed in the thermochemical and spectroscopic studies. The results presented the potential of the composites to produce SPI biopolymers with tannins and kraft lignin, leading to the development of multifunctional materials as an alternative for sustainable packaging.

Keywords: Soy Protein Isolate; Kraft Lignin; Tannins; Composite and blend; Casting technique.

Resumo

No presente estudo, bioplásticos multifuncionais isolados de proteína de soja (SPI) foram preparados por vazamento, com adição de taninos extraídos de *Stryphnodendron adstringens* e lignina kraft. Os filmes foram obtidos pelo método de compósitos e blends de biopolímeros, preparados em três pHs (8,5, 9,5 e 10,5) e caracterizados por estudos termoquímicos, espectroscopia de infravermelho com transformada de Fourier, microscopia eletrônica de varredura, permeabilidade ao vapor de água (WVP), atividade antioxidante, contato com água ângulo, energia de superfície, molhabilidade e testes mecânicos. Os compósitos apresentaram melhores resultados quando comparados aos filmes blenda e controle, respectivamente, nos testes de polaridade, hidrofobicidade, WVP e principalmente nos testes de atividade antioxidante. No entanto, nenhuma diferença significativa entre as amostras foi observada nos estudos termoquímicos e espectroscópicos. Os resultados apresentaram o potencial dos compósitos em produzir biopolímeros SPI com taninos e lignina kraft, levando ao desenvolvimento de materiais multifuncionais como alternativa para embalagens sustentáveis.

Palavras-chave: Isolado de proteína de soja; Kraft Lignina; Taninos; Composto e mistura; Técnica de fundição.

Resumen

En el presente estudio, se prepararon bioplásticos multifuncionales aislados de proteína de soja (SPI) mediante colada, con la adición de taninos extraídos de *Stryphnodendron adstringens* y lignina kraft. Las películas se obtuvieron mediante el método de biopolímeros compuestos y mezclas, preparadas a tres pHs (8.5, 9.5 y 10.5) y caracterizadas por estudios termoquímicos, espectroscopía infrarroja por transformada de Fourier, microscopía electrónica de barrido, permeabilidad al vapor de agua (WVP), actividad antioxidante, contacto con el agua. Ángulo, energía superficial, humectabilidad y ensayos mecánicos. Los composites presentaron mejores resultados cuando se compararon con las películas de mezcla y control, respectivamente, en las pruebas de polaridad, hidrofobicidad, WVP y especialmente en las pruebas de actividad antioxidante. Sin embargo, no se notó ninguna diferencia significativa entre las muestras en los estudios termoquímicos y espectroscópicos. Los resultados presentaron el potencial de los composites para producir biopolímeros SPI con taninos y lignina kraft, lo que llevó al desarrollo de materiales multifuncionales como alternativa para el envasado sostenible.

Palabras clave: Aislado de proteína de soja; Kraft Lignina; Taninos; Compuesto y mezcla; Técnica de fundición.

1. Introduction

Innovation is the successful exploration of new ideas, regarding a product and/or process, possibly resulting in lower costs of the processing, access to new markets, income increase, profit margin increase, among many benefits (Abgi, 2020). By analyzing this search for innovative products, it is possible to highlight macromolecules and biodegradable polymers such as SPI (Soy Protein Isolate).

SPI has been receiving visibility due to its application in various industrial settings, once it is capable of generating products/bioproducts, which favors sustainability and helps in a cycle-based economy view. Such subproduct presents advantages related to its biodegradability, biocompatibility and because it is obtained from renewable sources, for example, soy milk polysaccharides, diversified starches and oils (Arfat et al., 2014; Muller et al., 2011; Ortega-Toro et al., 2014; Menezes Filho et al., 2021) SPI consists of a promising class of biomaterials which appeals to researchers all around the world, since it is a sustainable alternative to traditional plastics or polymers derived from crude oil (Dufresne et al., 2017).

In addition to this raw material, the consequent interest in biomolecules such as lignin and tannins has been increasing, due to their biodegradability properties, renewable origin, industrial waste, market availability and low cost (Zhu et al., 2020; Gupta et al., 2020; Rajha et al., 2019). However, their commercial use is extremely limited, once such materials present mechanical, thermal and physicochemical properties that are not as good as those of products obtained from polymers derived from fossil sources (Cazón et al., 2017; Gopi et al., 2019). Despite their enormous potential, technologies that use lignin and/or tannins have not been completely developed, and the materials based on these biomolecules, especially residual lignin from the kraft process, and tannins from *Stryphnodendron adstringens* bark, have not been used to create products with high added value at industrial level (Sattler, 2019).

The interest in biopolymer films has been growing due to their various functions in the industrial sector, mainly regarding food packaging costs (Asgher et al., 2020). Such materials may be of renewable and sustainable origin, competing against the fossil product market. Overall, many strategies to promote improvements in the properties of these biodegradable films have been adopted, enabling studies on the commercial application of multifunctional packaging (Tayeb et al., 2020; Li et al., 2021; Zedeh et al., 2018; Laurichesse et al., 2014; Imre et al., 2013).

When it comes to packaging production, the casting method is commonly used to obtain bioplastics (Hossain et al., 2018). It is possible to obtain thin films (Zadeh et al., 2018; Ma et al., 2019; Monteanu et al., 2020) through techniques that use polymer blends and/or composites, by creating physical mixtures with polymer/biopolymer additives (combination of two or more biomolecules, such as tannins, lignin and SPI). The packaging technology field has been increasingly explored, in order to reach materials with greater antioxidant, flavoring, antimicrobial properties which do not absorb oxygen and present high commercial applicability, ensuring the multifunctionality of the final product (Vilas et al., 2020; Rehman et al., 2020; Zhong et al., 2020; Su et al., 2021; Coradi et al., 2020; Ajwani-Ramchandani et al., 2021).

Therefore, the aim of the present study is to develop thin films from soy protein isolate, kraft lignin and tannins, obtained by casting, using the concepts of polymer blends and composites. It is possible to decrease the degradability of the product wrapped by the final material by reaching a material with multifunctional characteristics, such as antioxidant activity, low water vapor permeability, low wettability, and high surface energy.

2. Materials and Methods

Reagents

The soy protein isolate (SPI) - (PROTIMARTI M90 IJ), with 91.60% dry basis protein, was obtained from Marsul Proteínas LTDA (Monte Negro/RS, BRA). The tannins (TAN) were obtained from the *Stryphnodendron* species, extracted at the Laboratory of Wood Anatomy at the Federal University of Lavras (Lavras/MG, BRA). The glycerol (90.0%) was purchased from Sigma Aldrich (Brazil) and the Commercial Absolute Ethyl Alcohol (99.5%) from NEON. The kraft lignin was donated by a paper and cellulose company, and the deionized water ($\rho > 18.2$ MΩ cm) was obtained by a Barnstead Nanopure Diamond^{TM} purification system (Thermo Fisher Scientific Inc, USA). To adjust pH, 0.1 Sodium Hydroxide (Dinâmica Ltda. Brazil) was used.

Preparation of the film-forming solution by casting control film (CF)

The films were prepared using the casting methodology with adaptations (Guerrero et al., 2011). First, the solvent for the film-forming solution was prepared with a hydroalcoholic solution with 20% ethyl alcohol. For the control film (CF), 5.0 g of SPI and 3.75 g of glycerol solution (90%) were weighed, and the volume was completed to 100 ml. Afterwards, the film-forming solution was stirred for 20 minutes at room temperature and then taken to water bath, under slow stirring at 80 °C for 30 minutes. After this step, the solution was cooled in an ice bath to ~ 25 °C. Later, pH was adjusted to 8.5, 9.5 and 10.5 with 0.1 Mol L^{-1} NaOH solution, distant from the SPI isoelectric point, identified as 1, 2 and 3, respectively (PAGLIONE et al., 2019). Then, the solutions were poured onto *Petri* dishes (290 mm × 280 mm × 50 mm) and dried at 25 °C room temperature for 12 hours. All films were kept at 50 ± 5% humidity and 23 ± 2 °C temperature for 24 hours before any characterization test.

Preparation of the film-forming solution by casting: blend (A) and composite (B)

To produce blends and composites, 4.25 g of SPI, 0.5 g of tannins, 0.25 g of kraft lignin and 3.75 g glycerol solution (90%) were weighed, and the volume was completed to 100 mL with hydroalcoholic solution of 20% ethyl alcohol. For the blend methodology (A), all solids were added in the beginning of the process, whereas for the composite methodology (B), the tannins and kraft lignin were added after the ice bath. The rest of the production process was performed as for the control film.

Characterization of films

Mechanical properties

The analysis of film thickness was performed by measuring 3 different points of the sample with the aid of a digital micrometer (0.0001mm precision; Mitutoyo Sul Americana, Suzano, SP, Brazil). The mechanical properties of the samples were measure in a texture analyzer (Stable Micro Systems, model TATX2i, England), according to ASTM D882-0219. Five repetitions were performed for each film composition, and the average values were reported. The samples were prepared in strips (100 mm x 10 mm), fixed on the probe support at their extremities at a separation speed of 2 mm.s^{-1} until it ruptured. A 1 kN load cell was used in order to classify the material properties and verify the structure integrity of the films. The values of traction resistance (σ_t), Young's modulus (E) and elongation at break (δ) were obtained in the traction trials. The trials were performed at constant room temperature.

The puncture test was performed with a texture analyzer (Stable Micro Systems, model TATX2i, England). The films were cut into 9 cm² squares and fixed on a support with a central orifice of 2.1 cm diameter. A spherical probe with 5.0 mm diameter (P/5S probe) was introduced perpendicularly to the surface of the film at constant speed of 0.8 mm/s until the probe punctured the film. The force at the rupture point (σ_{rp}, N) and the rupture point

deformation (ε_{rp}, mm) were calculated using the Exponent Lite Software (version 6.1.11.0, license no.: 5173-14273109-19689). Five specimens were tested for each film.

Thermogravimetric analysis (TGA) and differential scanning calorimetry (DSC)

The thermogravimetric analysis (TGA) looks for the breaking points of molecular interaction and material degradability at high temperatures. Such process was performed using a Q500 (TA Inc. New Castle, DE). Approximately 5.0 mg of the sample was heated from room temperature (25 °C) to 800 °C at a heating rate of 10 °C /min.$^{-1}$ under a nitrogen atmosphere (50 mL min.$^{-1}$). Each sample was tested three times and the average of the results was reported.

Differential scanning calorimetry (DSC) was performed using a Q100 (TA Instruments, New Castle, DE, USA). The 6.0 mg samples were subjected to heating/cooling/heating ramps with temperatures between -50 °C and 150 °C, at a 10 °C/min under nitrogen atmosphere. The glass transition temperature (Tg) and the melting temperature (Tm) of the samples were determined.

Attenuated total reflection (FTIR)

 The attenuated total reflection Fourier transform infrared spectroscopy (FTIR-ATR) of the films was measured with a *Bruker Alpha II* spectrophotometer. Samples from each film were used to perform 64 scans at the mid-infrared range (4000 to 400 cm^{-1}), with spectral resolution of 4 cm^{-1} to obtain spectra, in order to assess the main bonds detected in the structural formation of the biopolymer.

Scanning electron microscopy (SEM)

The samples with approximately 5 mm of thickness were placed on stubs with carbon adhesive tape and coated with gold, under vacuum conditions for 180 seconds. The LEO EVO 40 (Zeiss, Cambridge, England) with accelerating voltage of 10 kV was used to obtain the Scanning Electron Microscopy (SEM) micrographs. A surface and interior analysis of the samples via cryogenic fracture was performed to assess the properties and uniformity of the obtained film.

Water contact angle (WCA), surface energy (SE) and wettability (W)

Determination of water contact angle, wettability and surface energy was performed using a KRUSS Drop Shape Analyzer, model DSA 25B. The polar and dispersive contribution values for the surface energy (mN.m^{-1}) of the films were measured by the contact angles formed by distilled water, ethylene glycol, glycerol, 1-bromonaphthalene and diiodomethane. Wettability was obtained by measuring the contact angle formed by the drops of distilled water on the surface of the films at 5' and 60'. The water contact angle and the surface energy were obtained with the Advance software, using the Owens, Wendt, Rabel and Kaelble method (OWRK).

Evaluation of the antioxidant activity (DPPH)

The DPPH assay is based on the unstable free radical rate, in which the reactant 2,2-diphenyl-1-picrylhydrazyl (DPPH) forms a complex with itself and presents color. A 0.5 mL aliquot of the film extract solution was mixed with 3.5 mL of the DPPH methanol solution (25 mg L^{-1}), to assess the antioxidant properties of the obtained biopolymer (Tylewicz et al., 2020; Fasiku et al., 2020; Menezes Filho et al., 2022). The absorbance was measured at 517 nm after a 30 min. reaction in the dark room. The percentage of antioxidant activity (AA%) was calculated as follows:

$$AA\ (\%) = (A_{control} - A_{sample}) / (A_{control}) \times 100$$

Where: $A_{control}$ is the absorbance of the sample which only contains SPI (Tylewicz et al., 2020; Fasiku et al., 2020).

Assessment of the water vapor permeability (WVP)

The gravimetric method was used in the WVP test, according to ASTM E-96-16 (Guimarães et al., 2015). The film samples were sealed in amber glass capsules (film effective area of 0.000866 m^2) containing silica gel

(desiccant with 0% moisture). Afterwards, the capsules were placed in a desiccator at 25 °C and 75% relative humidity. The capsules were weighed periodically for 7 days at 24 h intervals.

WVTR and WVP were calculated from the data as follows:

$$TPVA = \Delta m / (A \times \Delta t)$$

$$PVA = TPVA \times \Phi / \Delta p$$

Where: WVTR is the water vapor transmission rate, and WVP is water vapor permeability. Δt is the capsule mass change over time (g x s^{-1}), A is the film effective area (m^2), Φ is film thickness (m) and Δp is the difference in water vapor partial between the films (Pa).

Statistical analysis

Variance analysis was used to analyze the results of the quantitative tests, and the averages were compared using the Scott-Knott test to evaluate significantly different averages with the SISVAR® software (Ferreira et al., 2019).

3. Results and Discussion

Film morphology (SEM)

Significant differences between morphological structures in the treatments may be observed in the fracture micrographs (Figure 01), given that the control films, the blends and composites presented greater, average and smaller cracks, respectively. Therefore, the addition of biomolecules to the film medium was relevant, once it altered the packaging properties and the homogeneity placement of samples.

The blends and composites presented less scratches and cracks when compared to the control film and at different pHs. In the 8.5 pH range, films presented better homogeneity overall, as seen in other studies (Kokoszka et al., 2010; Wang et al., 2017; Mauri et al., 2008; Nandane et al., 2015).

The analyses of film surface presented a homogeneous structure, without the presence of pores, which suggests an orderly packing of particles in the system for the proposed blend and composite methodologies when compared to the control film.
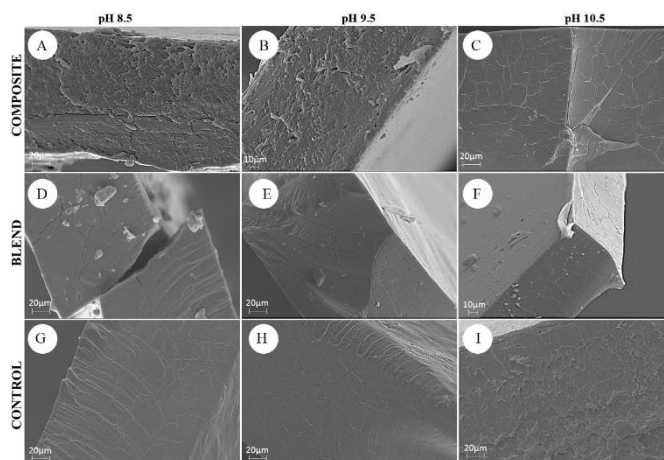
Figure 1. Micrographs of Fracture of the films at 1000x magnification. Source: Authors, 2021.

FTIR spectroscopy of films

For the spectra of the different treatments (Figure 02), a high similarity was observed between samples, with no different absorption bands appearing, even when the additives proposed in different methodologies were added. This result may be due to high rates of SPI matrix presence, without significant difference between samples (Yan et al., 2017; Wang et al., 2011).
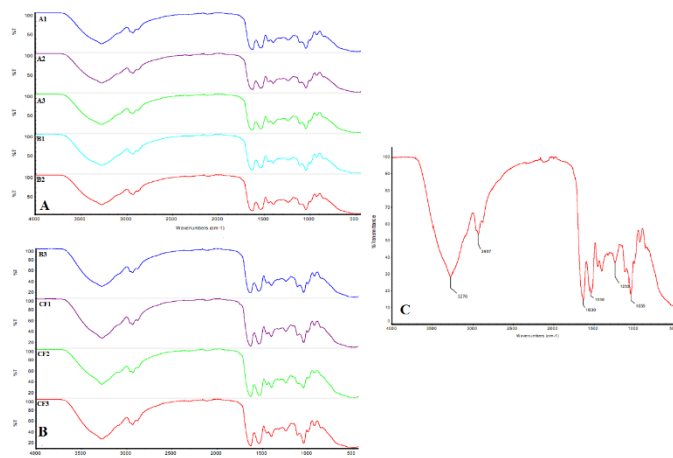
Figure 2. FTIR spectra of the films for different methodologies. Source: Authors, 2021.

Caption: Figure 2A: A1 = Blend Film pH 8.5; A2= Blend Film pH 9.5; A3= Blend Film pH 10.5; B1= Composite Film pH 8.5; B2= Composite Film pH 9.5. Figure 2B: B3= Composite Film pH 10.5; CF1= Control Film pH 8.5; CF2= Control Film pH 9.5; CF3= Control Film pH 10.5. Figure 2C: General spectrum sketch.

Nevertheless, the spectra of the samples presented characteristic peaks. The peak at 3270 cm^{-1} (O-H and N-H axial deformation stretching) is associated with O-H vibrations of the phenolic groups present in the tannin compounds, which contribute to the antioxidant activity of the material, and amine terminal of the protein (DE Souza et al., 2020; Wang et al., 2016). The one at 2937 cm^{-1} (C-H axial deformation), is related to the C-H band dislocation, a behavior that may demonstrate the relation between the matrix and its additives (Han et al., 2018).

The C=O axial deformation from amides I, which are characteristic of β sheets connected by hydrogen interactions in the PSI matrix, is shown by the peak at 1630 cm^{-1}. Such amides are abundant in thin films, as shown by studies that have reported the presence of processed globular proteins in their composition (Wang et al., 2018; Ciannamea et al., 2016; Arunkumar et al., 2019). The peaks at 1536-1233 cm^{-1} (C-N deformation or N-H angular deformation) are associated with vibrations of the aromatic ring present in macromolecules and in interactions between the matrix and its additives (Wang et al., 2016). The one at 1039 cm^{-1} may be related to the C-H deformation present in the hydrocarbon structures of the system, or to the C-O stretching, which is due to a slight dislocation of the glycerol bands (Han et al., 2018; Liu et al., 2017).

The FTIR analysis of the samples allowed the observation of bands that are characteristic of amide groups, mainly present in the protein structures derived from peptide bonds. It also allowed the observation of bands from carbonyl groups present in tannins and in the matrix, which possibly interact with the hydroxyl groups and amines present in the system and make amide I bonds possible (C-O stretching) (Arunkumar et al., 2019; Bocker et al., 2017; Kristoffersen et al., 2020).

Thermogravimetric analysis (TGA)

In the TGA, all samples presented 03 stages of mass loss (Table 01), where the first stage (30 °C to 190 °C) would correspond to loss of water and of organic acid residues (Liu et al., 2017), which would happen through the breaking of hydrogen bonds between the groups present in the system and hydroxyl groups. In such stage, the films showed a homogeneity in mass loss of approximately 10% for all samples (Qin et al., 2019; Jawerth et al., 2020).

Regarding the second stage (190 °C to 580 °C) the samples presented significant mass loss of approximately 60%. This loss is due to the degradation of glycerol, SPI matrix (Liu et al., 2017), and phenolic rings present in

the system, and to the decomposition of steroid groups through the breaking of amide bonds (Qin et al., 2019; Jawerth et al., 2020).

In the third stage (580 °C to 800 °C), mass loss referred to proteins (Liu et al., 2017; Qin et al., 2019; Jawerth et al., 2020), and composites and control films presented lower mass loss (2%) when compared to blends (~15%), as a result of the conjugation that occurs in the forming process of blends (Ivorra-Martinez et al., 2020; Ferri et al., 2020).

In this last stage, the temperature corresponds to carbonization, at which the films subjected to the analysis become residue. The composite films presented a higher rate of stable residues (approximately 25%) when compared to the control film (20%) and blends (15%). Such results may indicate that treatment A generates films that are more susceptible to degradation.

Table 1. Thermogravimetric analysis (TGA and DSC).

Treatments	TR (°C)	ML (%)	SR (%)	Tg (°C)	Tm (°C)
CF1	30 to 190	10.05	19.58	-38.46	93.72
	190 to 580	64.06			
	580 to 800	2.98			
CF2	30 to 190	10.60	20.15	-33.80	89.83
	190 to 580	65.67			
	580 to 800	2.64			
CF3	30 to 190	10.19	20.75	-36.18	82.32
	190 to 580	66.13			
	580 to 800	2.52			
A1	30 to 190	12.30	14.94	-36.40	82.31
	190 to 580	60.70			
	580 to 800	17.28			
A2	30 to 190	12.93	11.47	-35.96	79.43
	190 to 580	59.23			
	580 to 800	15.68			
A3	30 to 190	11.06	15.18	-35.21	74.85
	190 to 580	57.63			
	580 to 800	9.63			
B1	30 to 190	10.83	23.09	-36.74	82.72
	190 to 580	60.85			
	580 to 800	2.95			
B2	30 to 190	11.17	25.47	-36.65	83.72
	190 to 580	59.53			
	580 to 800	2.98			
B3	30 to 190	10.65	26.84	-35.43	83.43
	190 to 580	58.71			
	580 to 800	2.93			

CF1= Control Film ph 8.5; CF2= Control Film ph 9.5; CF3= Control Film ph 10.5; A1 = Blend Film ph 8.5; A2= Blend Film ph 9.5; A3= Blend Film pH 10.5; B1= Composite Film pH 8.5; B2= Composite Film pH 9.5; B3= Composite Film pH 10.5; TR= Temperature Range; ML= Mass Loss; SE= Stable Residue at 800 °C; Tg= Glass Transition Temperature; Tm= Crystalline Melting Temperature.

Differential scanning calorimetry (DSC)

The DSC curves show information about miscibility of the mixture components through the analysis of changes in melting temperature (Tm) and glass transition temperature (Tg) due to its composition (Blanco et al., 2017; De Souza et al., 2019; Boubekeur et al., 2020; Kiruthika et al., 2020), as seen in (Table 1).

It is worthy to mention that the samples underwent thermal degradation at approximately 150 °C, which led the experiment to perform only one heating ramp from -50 °C to 150 °C in order to assess their respective glass transition and melting temperatures.

In the DSC analysis, in which the glass transition temperatures (Tg) are approximately -36.0 °C and the melting temperatures (Tm) approximately 85.0 °C, sample homogeneity may be observed regardless of the treatment. Therefore, no significant evidence was seen among samples, which corroborates the spectroscopic results.

However, a small variation was found in Tm regarding pH values of each treatment, where the higher the pH, the lower the sample Tm. The decrease in temperature may be attributed to the interactions between the carbonyl groups and the hydroxyl (-OH) and amine ($-NH_2$) groups present in the system, causing a reduction of film crystallinity according to the treatments (Siddaiah et al., 2018; Mora et al., 2020; Huang et al., 2008; Chiu et al., 2011).

It has been reported that the increase in glycerol decreases Tg, once the polymer matrix becomes less dense and the addition of plasticizer promotes the mobility of polymer chains (Mali et al., 2006). Nonetheless, by comparing film Tgs, it was detected that the higher the pH, the lower the Tg (Chen et al., 2005; Tang et al., 2006). However, in this case, Tg increase is a result of a decrease in the space available for molecular motion.

Thus, the pH increase favored a greater microstate of molecules in the system (due to the solution adjustment), leading to an increase in the kinetic space of the microenvironment at the interaction level (Ray et al., 2018).

Polarity analysis of the films (WCA, SE and W)

The variance analysis showed that the factor treatment was significant ($p < 0.05$) for all variables in the polarity tests. The water contact angle (WCA), wettability (W) and surface energy (SE) may be observed in (Table 2).

By analyzing WCA along with W, it is possible to indicate the capability of the surface to moisten itself (Pradywong et al., 2017). An angle below 90° means a low surface tension, and the lower the wettability, the more hydrophobic the surface. Consequently, the films presented hydrophilic characteristics (< 90°), but the composites presented angles that were closer to hydrophobicity (Zhang et al., 2016), followed by the blends and the control film. Studies have reported that depending on the kind of solvent used, there is a significant influence on film properties when the film contains lignin (Alwadani et al., 2021).

Due to the pH increase in the system, there is an increase in sample hydrophobicity, when compared within the same treatment. Nevertheless, when it comes to W, the films did not show a great difference in results, presenting low coefficients. However, the composites had a better performance, showing an increase in surface hydrophobicity, which may contribute to a higher antioxidant capacity (Laguerre et al., 2010) when compared to the blends and especially to the control film, respectively (Qin et al., 2019).

The evidence obtained with WCA and W (Li et al., 2017) was confirmed through the SE test, in which the rates of apolar components could be assessed when the film was exposed to various polar and apolar agents and its combination resulted in the SE rates of samples (Table 1). Therefore, by analyzing the column of apolar character, it was possible to observe that the composite treatment has a greater hydrophobic SE, followed by the blends, and then the control film, possibly due to the hydrogen bonds between the SPI and the additives (Liu et al., 2017; Alwadani et al., 2021).

Thus, the addition of charges influences hydrophobicity of films, promoting an improvement in their properties, favoring repulsion of polar molecules and making the material less hydrophilic, which is convenient to the packaging market (Amparo et al., 2020; Wang et al., 2020; Bhadra et al., 2020).

Table 2. Water contact angle analysis, wettability, surface energy analysis and hydrophobicity.

Treatments	*t* (mm)	WCA [°]	W [°]	SE [mN/m]	SE [mN/m] Dispersion	SE [mN/m] Water	SE [mN/m] 1-Bromonaphthalene	SE [mN/m] Diiodomethane	SE [mN/m] Ethylene glycol	SE [mN/m] Glycerol
CF1	0.211 ± 0.96 a	59.32 ± 0.49 a	0.06 ± 0.02 a	33.94 ± 0.66 a	20.32 ± 0.31 a	70.23 ± 0.37 a	44.28 ± 0.67 a	56.26 ± 0.59 a	58.97 ± 0.34 a	75.76 ± 2.61 a
CF2	0.213 ± 0.84 a	48.38 ± 0.73 c	0.15 ± 0.03 c	40.04 ± 0.93 c	20.50 ± 0.39 c	47.00 ± 0.27 e	50.06 ± 1.21 a	54.40 ± 0.08 b	45.40 ± 0.68 e	88.90 ± 0.81 a
CF3	0.212 ± 0.87 a	39.84 ± 0.39	0.08 ± 0.01 b	42.17 ± 0.94 b	20.27 ± 0.59 c	63.58 ± 0.78 b	50.39 ± 0.66 a	54.82 ± 0.91 b	46.21 ± 0.66 e	85.17 ± 1.91 b
A1	0.122 ± 0.65 b	56.41 ± 0.98 b	0.09 ± 0.03 b	29.31 ± 0.85 b	24.04 ± 0.10 b	65.49 ± 1.10 b	51.02 ± 0.12 a	47.48 ± 0.41 b	67.42 ± 0.68 a	83.39 ± 0.68 c
A2	0.125 ± 0.59 b	57.91 ± 0.87 b	0.09 ± 0.01 b	40.19 ± 0.39 c	25.62 ± 0.86 b	53.59 ± 0.55 b	50.84 ± 0.27 a	47.79 ± 0.38 f	55.58 ± 1.06 c	83.40 ± 1.39 c
A3	0.123 ± 0.51 b	59.19 ± 0.74 b	0.13 ± 0.03 c	45.05 ± 0.87 a	24.68 ± 0.41 b	48.01 ± 0.72 e	50.52 ± 0.72 a	53.12 ± 0.93 c	56.11 ± 0.83 c	79.55 ± 1.24 d
B1	0.135 ± 0.53 c	67.32 ± 0.53 a	0.06 ± 0.03 a	38.73 ± 0.78 d	30.41 ± 0.60 a	59.78 ± 0.57 c	48.27 ± 0.11 b	50.63 ± 0.52 d	57.65 ± 0.72 b	82.79 ± 1.84 c
B2	0.133 ± 0.51 c	66.67 ± 0.99 a	0.10 ± 0.01 c	49.17 ± 0.96 a	30.28 ± 0.69 a	55.77 ± 0.31 d	48.52 ± 0.90 b	49.23 ± 0.34 e	57.04 ± 0.98 b	83.58 ± 1.13 c
B3	0.136 ± 0.58 c	64.56 ± 0.65 a	0.05 ± 0.02 a	43.45 ± 0.53 b	30.52 ± 0.46 a	53.68 ± 0.77 d	42.65 ± 0.41 d	50.51 ± 0.42 d	51.43 ± 0.91 d	83.78 ± 1.48 c

[a, b, c, d, e, f] Averages observed in columns with the same letter do not differ statistically according to the Scott-Knott test (p<0.05). CF1= Control Film pH 8.5; CF2= Control Film pH 9.5; CF3= Control Film pH 10.5; A1 = Blend Film pH 8.5; A2= Blend Film pH 9.5; A3= Blend Film pH 10.5; B1= Composite Film pH 8.5; B2= Composite Film pH 9.5; B3= Composite Film pH 10.5; *t* = Sample Thickness; WCA= Water Contact Angle; W= Wettability; SE= Surface Energy. Trea = Treatments. Source: Authors, 2021.

Table 3. Mechanical properties, water vapor permeability and evaluation of the antioxidant activity.

Trea	t (mm)	E (Mpa)	δ (%)	σ_{tr} (Mpa)	σ_{rp} (N)	ε_{rp} (mm)	WVP $(g/Pa \cdot s \cdot m^2)10^7$	DPPH (%)
CF1	0.211 ± 0.96 [a]	28.681 ±1.57 [c]	93.234 ± 1.37 [b]	2.053 ± 0.03 [c]	11.734 ± 0.39 [c]	09.535 ± 0.69 [b]	6.43 ± 0.24 [a]	25.85 ± 0.98 [a]
CF2	0.213 ± 0.84 [a]	19.896 ± 1.32 [d]	97.022 ± 1.47 [b]	1.560 ± 0.07 [d]	11.047 ± 0.48 [c]	07.099 ± 0.53 [c]	6.82 ± 0.66 [a]	27.49 ± 0.43 [c]
CF3	0.212 ± 0.87 [a]	15.240 ± 1.56 [d]	108.19 ± 1.85 [a]	2.204 ± 0.10 [c]	14.342 ± 0.74 [b]	12.857 ± 0.29 [a]	6.97 ± 0.32 [a]	31.58 ± 0.73 [f]
A1	0.122 ± 0.65 [b]	46.692 ± 1.21 [b]	82.904 ± 2.14 [c]	3.099 ± 0.18 [b]	13.214 ± 0.19 [b]	08.182 ± 0.12 [b]	3.41 ± 0.45 [b]	60.63 ± 0.45 [d]
A2	0.125 ± 0.59 [b]	44.556 ± 1.86 [b]	85.835 ± 1.33 [c]	3.387 ± 0.19 [b]	12.855 ± 0.54 [b]	09.155 ± 0.78 [b]	3.68 ± 0.29 [b]	69.87 ± 0.52 [c]
A3	0.123 ± 0.51 [b]	40.035 ± 1.49 [b]	68.051 ± 2.58 [e]	3.144 ± 0.47 [b]	18.228 ± 0.83 [a]	10.902 ± 0.43 [b]	3.63 ± 0.06 [b]	71.46 ± 0.44 [b]
B1	0.135 ± 0.53 [c]	58.079 ± 1.02 [a]	81.262 ± 1.73 [c]	3.752 ± 0.19 [a]	08.401 ± 0.29 [d]	05.174 ± 0.28 [d]	1.83 ± 0.38 [c]	57.63 ± 0.61 [e]
B2	0.133 ± 0.51 [c]	55.254 ± 1.09 [a]	75.448 ± 1.50 [d]	3.871 ± 0.35 [a]	07.590 ± 0.87 [d]	05.527 ± 0.37 [d]	1.92 ± 0.28 [c]	60.37 ± 0.64 [d]
B3	0.136 ± 0.58 [c]	50.721 ± 1.07 [a]	73.006 ± 0.80 [d]	3.994 ± 0.14 [a]	16.583 ± 0.86 [a]	08.312 ± 0.94 [b]	2.02 ± 0.33 [c]	73.47 ± 0.29 [a]

[a, b, c, d, e, f, g, h] Averages observed in columns with the same letter do not differ statistically according to the Scott-Knott test (p<0.05). CF1= Control Film pH 8.5; CF2= Control Film pH 9.5; CF3= Control Film pH 10.5; A1 = Blend Film pH 8.5; A2= Blend Film pH 9.5; A3= Blend Film pH 10.5; B1= Composite Film pH 8.5; B2= Composite Film pH 9.5; B3= Composite Film pH 10.5; t = Film Thickness; σ_{tr} = Traction Resistance; δ = Elongation; E = Young's Modulus; σ_{rp} = Force at the Rupture Point; ε_{rp} = Rupture Point Deformation; WVP= Water Vapor Permeability; DPPH= Antioxidant Activity. Trea = Treatments. Source: Authors, 2021

Mechanical properties of the films

The variance analysis showed that the factor treatment was significant ($p < 0.05$) for all variables in the mechanical studies. Traction resistance (σ_t), elongation (δ), Young's modulus (E), force at the rupture point (σ_{rp}) and rupture point deformation (ε_{rp}) are represented in (Table 3).

The adjustment of pH towards a more alkaline medium caused an increase in sample stretch (δ), regardless of the treatment. Besides, it caused a lower interaction of intermolecular bonds; consequently, decreasing E and homogenizing samples regarding σ_t. When it came to σ_t and E, the composites stood out considerably when compared to the blends and CFs regarding film treatments. Polymerization normally helps to form a net that potentially reduces elongation and increases σ_t, thus improving general mechanical properties (Zhang et al., 2016; Kumar et al., 2014).

The increase in TR and E in the composites may be due to the effective transference of the matrix tension to the particles, which leads to improved mechanical properties (Peng et al., 2018), as seen in the micrographs of the B films. Such characteristics stem from a greater flexibility of the chain and difficulty in regular or ordered packing of films, with main characteristics of an amorphous phase attributed to hydrogen bonds and to the structures obtained through the load of additives applied and the matrix (Zhang et al., 2016).

It is possible to observe this same behavior on biodegradable hybrid composites based on a biopolymer matrix and reinforced with lignin, in which they showed increased sample σ_t and E (Kumar et al., 2014; Bassyouni et al., 2017). Regarding the E, which describes material stiffness, the values of composites presented an increase when compared to the blends and CF, respectively. Thus, it showed that CFs would be more flexible, which favors energy recovery and absorption in the elastic deformation of the film subjected to the test.

When it comes to elongation, the blends demonstrated a better result, generating a more ductile material than the composites, though inferior to the control film. The addition of biomolecules loads was not interesting to elongation at break except at pH 10.5, in which the composite presented a significant increase regarding the blend of equal pH. Similar studies state that the addition of Rutin (a biomolecule similar to tannins) to the protein films produced a more compact structure, due to possible interactions between the phenolic compound and the soy proteins (Friesen et al., 2015).

In the puncture analysis, the blends stood out regarding σ_{rp} and ε_{rp} when compared to the other treatments, showing a greater intermolecular interaction happened in their processing and, consequently, resulted better mechanical properties, as seen in studies. The composites, on the other hand, presented a lower σ_{rp} and ε_{rp} rate, demonstrating that the addition of loads did not yield an improvement in puncture tests.

Water vapor permeability (WVP)

The water vapor permeability value of the SPI film is a very important feature for food packaging (Wang et al., 2016). The WVP values of the pure SPI films and of both treatments (blend and composite) are shown in Table 03.

The addition of loads to the film-forming solution, especially of polyphenolic additives may increase tortuosity in the diffusion of water vapor molecules, hindering their passage through the film. Therefore, it can increase the water resistance properties of a biopolymer film, a technique that is widely used in the packaging industry (Wang et al., 2014; Koshy et al., 2015).

There was no significant difference in the WVP values for the different pHs evaluated (8.5; 9.5; 10.5). Such result differs from the data observed in the literature, which states that the higher the alkalinity of the medium, the more hydrophobic the film, thus causing a decrease in the WVP rate (Jiang et al., 2012). Nonetheless, for the blend and composite methodologies, it was possible to observe a decrease of approximately 6.7 g/Pa.s.m² in WVP for the control film, approximately 3.5 g/Pa.s.m² for the blends and 1.9 g/Pa.s.m² for the composites (Siracusa et al., 2012), favoring the comparison between this B film commercial plastics/bioplastics. This decrease in WVP was previously reported in other protein systems caused by the addition of polyphenolic compounds, such as gelatin films made with thyme, propolis, myrtle, citrus and green tea extracts (Ciannamea et al., 2016), forming a more compact structure.

Consequently, the control film which only contains the SPI matrix has a higher fracture rate, allowing a greater passage of gaseous molecules, as seen in Figure 02. The intermolecular interactions lead to an increase of the spaces between soy protein polymer chains, which elevates water molecule mobility in the matrix, therefore favoring the migration of water through the control film (Li et al., 2021).

The preparation and dispersion method determines the nature of the system for blends or composites. The interaction between the matrix and the additives is of physical nature for the blends system, while for the composites; this interaction may involve chemical interactions (Bhadra et al., 2020). The kind of system formed will interfere in the water vapor transmission, which involves adhesion and diffusion of water molecules in the film matrix.

Thus, the presence of additives of hydrophobic nature in the composites hindered the diffusion of water molecules through the matrix, granting them low WVP rates. Therefore, the composites present a higher structural packing level, favoring a better longitudinal distribution, which leads to a transverse state with less ruptures and allows for an extremely low WVP rate in the system.

Antioxidant activity (DPPH)

Antioxidant activity, also known as DPPH analysis, measures the compound capacity to eliminate the radical (or donate/transfer a hydrogen) through the present antioxidant. It is important to highlight that components such as pH, metal ions, and solvent incubation and reaction periods may influence the reaction (Chen et al., 2020). Consequently, if there is a test limitation, it may be connected to the interaction with other radicals present, such as alkyl groups.

As seen in Figure 3 and Table 3, after the addition of loads in both the blend and composite methodologies, DPPH rates increased, displaying a slightly higher capacity to eliminate radicals than the control films. Such difference can be attributed to the high compatibility of the additives in the protein matrix, favoring the antioxidant activity of the medium (Zadeh et al., 2018; Cano et al., 2020; Mohanan et al., 2018).

Figure 3. Graph correspondent to the DPPH antioxidant activity in the samples.
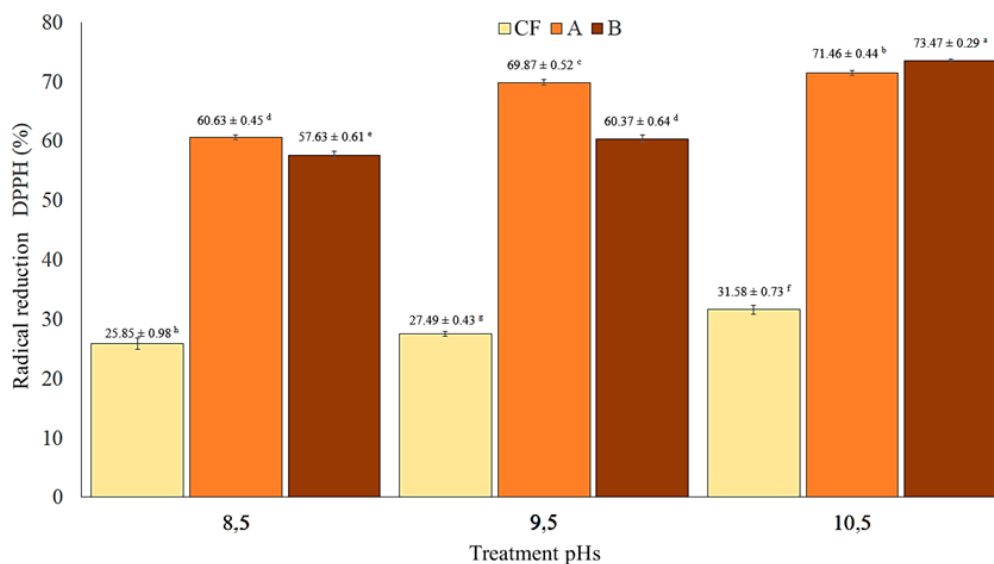
Note: a, b, c, d, e, f Averages observed in columns with the same letter do not differ statistically according to the Scott-Knott test (p < 0.05). CF1= Control Film pH 8.5; CF2= Control Film pH 9.5; CF3= Control Film pH 10.5; A1 = Blend Film pH 8.5; A2= Blend Film pH 9.5; A3= Blend Film pH 10.5; B1= Composite Film pH 8.5; B2= Composite Film pH 9.5; B3= Composite Film pH 10.5

The loads of biomolecules added to the SPI samples (films A and B), are groups of phenolic compounds soluble in water that present antioxidant activity. This characteristic is linked to their structure and redox property, which is a relevant feature for the neutralization of free radicals. Furthermore, tannin-protein interaction occurs in tannin-based films, meaning the phenolic compound is confined and cannot spread. This way, antioxidant activities are greater regarding films that do not contain the additive (Mohanan et al., 2018).

The antioxidant capacity of the control film might be related to the antioxidant action of the amino acids with phenolic side chains, such as phenylalanine, tyrosine and tryptophan, and phenolic compounds, such as

isoflavones and chlorogenic, caffeic and ferulic acids present in the SPI which are strong free radical scavengers (Ma et al., 2019; De Souza et al., 2020; Wang et al., 2016; Ciannamea et al., 2016).

Among the hydrophilic antioxidants, tannic acid presents the highest capacity to eliminate free radicals (ex: singlet oxygen, OH$^-$ and H$_2$O$_2$,), followed by caffeic and ascorbic acids (Chen et al., 2020; Menezes Filho et al., 2022). This might also be observed in this study due to the presence of kraft lignin, which may increase the activity of free radical elimination in the system by 55% (Zadeh et al., 2018).

4. Conclusions

The addition of additives favored the multifunctional properties of the obtained bioplastics. The use of kraft lignin and tannins led to significant modifications in the morphology, hydrophobicity, and permeability of films. It also led to changes in the mechanical studies and especially in the antioxidant activity of composite films. On the other hand, composite films did not significantly stand out in the thermochemical and spectroscopic trials, due to the low concentration of additives in the bioplastic.

The methodology of composite films showed the best potential, with great antioxidant activity and water vapor permeability potential, meeting the objectives of this study, which were to produce multifunctional biopolymers with SPI, tannins and kraft lignin. Besides having the capacity to meet various high-performance research specifications, the composites methodology presented great technological innovation potential to be applied in the food industry.

5. Acknowledgments

6. References

Abgi. (2020). Accelerating Innovation. Gestão de projetos de inovação. *Accel Innov Gestão Proj Inovação*. https://brasil.abgi-group.com/o-que-fazemos/gestao-projetos-inovacao/.

Ajwani-Ramchandani, R., Figueira, S., Oliveira R. T., Jha, S., Ramchandani, A., Schuricht, L. (2021). Towards a circular economy for packaging waste by using new technologies: The case of large multinationals in emerging economies. *J Clean Prod*, *281*, 125139. https://doi.org/10.1016/j.jclepro.2020.125139.

Alwadani, N., Ghavidel, N., Fatehi, P. (2021). Surface and interface characteristics of hydrophobic lignin derivatives in solvents and films. Colloids Surfaces A Physicochem *Eng Asp*, *609*, 125656. https://doi.org/10.1016/j.colsurfa.2020.125656.

Amparo, L., Blanco-Padilla, A., Oksman, K. (2020). Strategies to Improve the Properties of Amaranth Protein Isolate-Based Thin Films for Food Packaging Applications : Nano-Layering through Spin-Coating and Incorporation of Cellulose Nanocrystals.

Arfat, Y. A., Benjakul, S., Prodpran, T., Sumpavapol, P., Songtipya, P. (2014). Properties and antimicrobial activity of fish protein isolate/fish skin gelatin film containing basil leaf essential oil and zinc oxide nanoparticles. *Food Hydrocoll*, *41*, 265–73. https://doi.org/10.1016/j.foodhyd.2014.04.023

Arunkumar, R., Drummond, C. J., Greaves, T. L. (2019). FTIR spectroscopic study of the secondary structure of globular proteins in aqueous protic ionic liquids. *Front Chem, 7*. https://doi.org/10.3389/fchem.2019.00074.

Asgher, M., Qamar, S. A., Bilal, M., & Iqbal, H. M. N. (2020). Bio-based active food packaging materials: Sustainable alternative to conventional petrochemical-based packaging materials. *Food Res Int*, *137*. https://doi.org/10.1016/j.foodres.2020.109625.

Bassyouni, M., Javaid, U., Hasan S. W. U. (2017). Bio-based hybrid polymer composites: A sustainable high performance material. Elsevier Ltd. https://doi.org/10.1016/B978-0-08-100789-1.00002-2.

Bhadra, J., Alkareem, A., Al-Thani, N. (2020). A review of advances in the preparation and application of polyaniline based thermoset blends and composites. *J Polym Res*, *27*.

https://doi.org/10.1007/s10965-020-02052-1.

Blanco, I., Cicala, G., Latteri, A., Saccullo, G., El-Sabbagh, A. M. M., Ziegmann, G. (2017). Thermal characterization of a series of lignin-based polypropylene blends. *J Therm Anal Calorim*, *127*, 147–53. https://doi.org/10.1007/s10973-016-5596-2.

Böcker, U., Wubshet, S. G., Lindberg, D., Afseth, N. K. (2017). Fourier-transform infrared spectroscopy for characterization of protein chain reductions in enzymatic reactions. *Analyst*, *142*, 2812-8. https://doi.org/10.1039/c7an00488e.

Boubekeur, B., Belhaneche-Bensemra, N., Massardier, V. (2020). Low-Density Polyethylene/Poly(Lactic Acid) Blends Reinforced by Waste Wood Flour. *J Vinyl Addit Technol*, *26*, 443-451. https://doi.org/10.1002/vnl.21759.

Cano, A, Andres, M., Chiralt, A., González-Martinez, C. (2020). Use of tannins to enhance the functional properties of protein based films. *Food Hydrocoll*, *100*. https://doi.org/10.1016/j.foodhyd.2019.105443.

Cazón, P., Velazquez, G., Ramírez J. A., Vázquez, M. (2017). Polysaccharide-based films and coatings for food packaging: A review. *Food Hydrocoll*, *68*, 136-148. https://doi.org/10.1016/j.foodhyd.2016.09.009.

Ciannamea, E. M., Stefani, P. M., Ruseckaite, R. A. (2016). Properties and antioxidant activity of soy protein concentrate films incorporated with red grape extract processed by casting and compression molding. *LWT - Food Sci Technol*, *74*, 353-362. https://doi.org/10.1016/j.lwt.2016.07.073.

Chen, P., Zhang, L. (2005). New evidences of glass transitions and microstructures of soy protein plasticized with glycerol. *Macromol Biosci*, *5*, 237–45. https://doi.org/10.1002/mabi.200400179.

Chen, X., Liang, L., Han, C. (2020). Borate suppresses the scavenging activity of gallic acid and plant polyphenol extracts on DPPH radical: A potential interference to DPPH assay. *Lwt*, *131*, 109769. https://doi.org/10.1016/j.lwt.2020.109769.

Chen, Y., Yan, Z., Liang, L., Ran, M., Wu, T., Wang, B. (2020). Comparative evaluation of organic acid pretreatment of eucalyptus for kraft dissolving pulp production. *Materials (Basel)*, *13*. https://doi.org/10.3390/ma13020361.

Chiu, M., Prenner, E. (2011). Differential scanning calorimetry: An invaluable tool for a detailed thermodynamic characterization of macromolecules and their interactions. *J Pharm Bioallied Sci*, *3*, 39–59. https://doi.org/10.4103/0975-7406.76463.

Coradi, P. C., Lima, R. E., Padia, C. L., Alves, C. Z., Teodoro, P. E., Cândido, A. C. S. (2020). Soybean seed storage: Packaging technologies and conditions of storage environments. *J Stored Prod Res, 89*, 101709. https://doi.org/10.1016/j.jspr.2020.101709.

De Sousa, R. R., Gouveia, J. R., Nacas, A. M., Tavares, L. B., Ito, N. M., De Moura, E. N., et al. (2019). Improvement of polypropylene adhesion by Kraft Lignin Incorporation. *Mater Res*, *22*. https://doi.org/10.1590/1980-5373-MR-2018-0123.

De Souza, K. C., Correa, L.G., da Silva, T. B. V., Moreira, T. F. M., de Oliveira, A., Sakanaka, L. S., et al. (2020). Soy Protein Isolate Films Incorporated with Pinhão (Araucaria angustifolia (Bertol.) Kuntze) Extract for Potential Use as Edible Oil Active Packaging. *Food Bioprocess Technol*, *13*, 998–1008. https://doi.org/10.1007/s11947-020-02454-5.

Dufresne, A., Castaño J. (2017). Polysaccharide nanomaterial reinforced starch nanocomposites: A review. *Starch/Staerke*, *69*,1-19. https://doi.org/10.1002/star.201500307.

Fasiku (Oluwaseun), V., Omolo, C. A., Govender, T. (2020). Free radical-releasing systems for targeting biofilms. *J Control Release*, *322*, 248–73. https://doi.org/10.1016/j.jconrel.2020.03.031.

Ferreira, D. F. (2019). Sisvar: a Computer Analysis System To Fixed Effects Split Plot Type Designs. *Rev Bras Biometria*, *37*, 529. https://doi.org/10.28951/rbb.v37i4.450.

Ferri, J. M., Garcia-Garcia, D., Rayón, E., Samper, M. D., Balart, R. (2020). Compatibilization and characterization of polylactide and biopolyethylene binary blends by non-reactive and reactive compatibilization approaches. *Polymers (Basel)*, *12*. https://doi.org/10.3390/POLYM12061344

Friesen, K., Chang, C., Nickerson, M. (2015). Incorporation of phenolic compounds, rutin and epicatechin, into soy protein isolate films: Mechanical, barrier and cross-linking properties. *Food Chem*, *172*, 18–23. https://doi.org/10.1016/j.foodchem.2014.08.128.

Gopi, S., Loganathan, G. B., Sekar, B. K., Krishnamoorthy, R. K., Sekaran, V., Mohan, A. R. (2019). Influence of water absorption on glass fibre reinforced IPN composite pipes. *Polimeros, 29*, 1–8. https://doi.org/10.1590/0104-1428.02818.

Guerrero, P., Stefani, P. M., Ruseckaite, R. A., De La Caba, K. (2011). Functional properties of films based on soy protein isolate and gelatin processed by compression molding. *J Food Eng*, *105*, 65-72. https://doi.org/10.1016/j.jfoodeng.2011.02.003.

Guimarães, M., Botaro, V. R., Novack, K. M., Teixeira, F. G., Tonoli, G. H. D. (2015). High moisture strength of cassava starch/polyvinyl alcohol-compatible blends for the packaging and agricultural sectors. *J Polym Res, 22*. https://doi.org/10.1007/s10965-015-0834-z.

Gupta, A. K., Tulsyan, S., Thakur N., Sharma, V., Sinha, D. N., Mehrotra, R.(2020). Chemistry, metabolism and pharmacology of carcinogenic alkaloids present in areca nut and factors affecting their concentration. *Regul Toxicol Pharmacol, 110*, 104548. https://doi.org/10.1016/j.yrtph.2019.104548.

Han, Y., Yu, M., Wang, L. (2018). Preparation and characterization of antioxidant soy protein isolate films incorporating licorice residue extract. *Food Hydrocoll*, *75*, 13–21. https://doi.org/10.1016/j.foodhyd.2017.09.020.

Hossain, K. M. Z., Felfel, R. M., Ogbilikana, P. S., Thakker, D., Grant, D. M., Scotchford, C. A., et al. (2018). Single Solvent-Based Film Casting Method for the Production of Porous Polymer Films. *Macromol Mater Eng, 303*, 1–7. https://doi.org/10.1002/mame.201700628.

Huang, J., Wigent, R. J., Schwartz, J. B. (2008). Drug-polymer interaction and its significance on the physical stability of nifedipine amorphous dispersion in microparticles of an ammonio methacrylate copolymer and ethylcellulose binary blend. *J Pharm Sci*, *97*, 251-262. https://doi.org/10.1002/jps.21072.

Imre, B., Pukánszky, B. (2013). Compatibilization in bio-based and biodegradable polymer blends. *Eur Polym J*, *49*, 1215-1233. https://doi.org/10.1016/j.eurpolymj.2013.01.019.

Ivorra-Martinez, J., Verdu, I., Fenollar, O., Sanchez-Nacher, L., Balart, R., Quiles-Carrillo, L. (2020). Manufacturing and properties of binary blend from bacterial polyester poly(3-hydroxybutyrate-co-3-hydroxyhexanoate) and poly(caprolactone) with improved toughness. *Polymers (Basel)*, *12*. https://doi.org/10.3390/POLYM12051118.

Jawerth M. E., Brett, C. J., Terrier, C., Larsson, P. T., Lawoko, M., Roth, S. V., et al. (2020). Mechanical and Morphological Properties of Lignin-Based Thermosets. *ACS Appl Polym Mater*, *2*, 668-676. https://doi.org/10.1021/acsapm.9b01007.

Jiang, J., Xiong, Y. L., Newman, M. C., Rentfrow, G. K. (2012). Structure-modifying alkaline and acidic pH-shifting processes promote film formation of soy proteins. *Food Chem, 132*, 1944-1950. https://doi.org/10.1016/j.foodchem.2011.12.030.

Kiruthika, S., Malathi, M., Selvasekarapandian, S., Tamilarasan, K., Maheshwari, T. (2020). Conducting biopolymer electrolyte based on pectin with magnesium chloride salt for magnesium battery application. *Polym Bull*, *77*, 6299-6317. https://doi.org/10.1007/s00289-019-03071-9.

Kokoszka, S., Debeaufort, F., Hambleton, A., Lenart, A., Voilley, A. (2010). Protein and glycerol contents affect physico-chemical properties of soy protein isolate-based edible films. *Innov Food Sci Emerg Technol*, *11*, 503-510. https://doi.org/10.1016/j.ifset.2010.01.006.

Kristoffersen, K. A., Van Amerongen, A., Böcker, U., Lindberg, D., Wubshet, S. G., De Vogel-Van Den Bosch, H., et al. (2020). Fourier-transform infrared spectroscopy for monitoring proteolytic reactions using dry-films treated with trifluoroacetic acid. *Sci Rep, 10*, 1-10. https://doi.org/10.1038/s41598-020-64583-3.

Koshy, R. R., Mary, S. K., Thomas, S., Pothan, L. A. (2015). Environment friendly green composites based on soy protein isolate - A review. *Food Hydrocoll*, *50*, 174–92. https://doi.org/10.1016/j.foodhyd.2015.04.023.

Kumar Thakur, V., Kumari Thakur, M., Raghavan, P., Kessler M. R. (2014). Progress in Green Polymer Composites from Lignin for Multifunctional Applications: A Review. *ACS Sustain Chem & Eng*, *2*, 1072–1092. https://doi.org/10.1021/sc500087z.

Laguerre, M., Giraldo, L. J., Lecomte, J., Figueroa-Espinoza, M. C., Baréa, B., Weiss, J., et al. (2010). Relationship between hydrophobicity and antioxidant ability of "phenolipids" in emulsion: A parabolic effect of the chain length of rosmarinate esters. *J Agric Food Chem*, *58*, 2869-2876. https://doi.org/10.1021/jf904119v.

Laurichesse, S., Avérous, L. (2014). Chemical modification of lignins: Towards biobased polymers. *Prog Polym Sci*, *39*, 1266–90. https://doi.org/10.1016/j.progpolymsci.2013.11.004.

Li, K., Jin, S., Chen, H., He, J., Li, J. (2017). A high-performance Soy protein isolate-based nanocomposite film modified with microcrystalline cellulose and Cu and Zn nanoclusters. *Polymers (Basel)*, *9*. https://doi.org/10.3390/polym9050167.

Li, J., Jiang, S., Wei, Y., Li, X., Shi, S. Q., Zhang, W., et al. (2021). Facile fabrication of tough, strong, and biodegradable soy protein-based composite films with excellent UV-blocking performance. *Compos Part B Eng*, *211*, 108645. https://doi.org/10.1016/j.compositesb.2021.108645

Li, T., Xia, N., Xu, L., Zhang, H., Zhang, H., Chi, Y., et al. (2021). Preparation, characterization and application of SPI-based blend film with antioxidant activity. *Food Packag Shelf Life*, *27*, 100614. https://doi.org/10.1016/j.fpsl.2020.100614.

Liu, X., Song, R., Zhang, W., Qi, C., Zhang, S., Li, J. (2017) Development of eco-friendly soy protein isolate films with high mechanical properties through HNTs, PVA, and PTGE synergism effect. *Sci Rep*, *7*. https://doi.org/10.1038/srep44289.

Ma, Q., Liang, S., Xu, S., Li, J., Wang L. (2019). Characterization of antioxidant properties of soy bean protein-based films with Cortex Phellodendri extract in extending the shelf life of lipid. *Food Packag Shelf Life*, *22*, 100413. https://doi.org/10.1016/j.fpsl.2019.100413.

Mali, S., Grossmann, M. V. E., García, M. A., Martino, M. N., Zaritzky, N. E.(2006). Effects of controlled storage on thermal, mechanical and barrier properties of plasticized films from different starch sources. *J Food Eng*, *75*, 453–60. https://doi.org/10.1016/j.jfoodeng.2005.04.031.

Mauri, A. N., Añón, M. C. (2008) Mechanical and physical properties of soy protein films with pH-modified microstructures. *Food Sci Technol Int*, *14*, 119-125. https://doi.org/10.1177/1082013208092130.

Menezes Filho, A. C. P., Oliveira Filho, J. G., Porfiro, C. A. (2021). Development and evaluation of a biodegradable packaging from the aryl of the fruit of Hymenaea stigonocarpa Mart. ex Hayne. *Sci Elec Arch*, *14*, 11-18. https://doi.org/10.36560/14820211322

Menezes Filho, A. C. P., Ventura, M. V. A., Alves, I., Taques, A. S., Batista-Ventura, H. R. F., Castro, C. F. S., Teixeira, M. B., Soares, F. A. L. (2022). Phytochemical prospection, total flavonoids and total phenolic and antioxidant activity of the mushroom extract *Scleroderma verrucosum* (Bull.) Pers. *Brazilian Journal of Science*, *1*(1), 1-7.

Menezes Filho, A. C. P., Ventura, M. V. A., Castro, C. F. S., Taques, A. S., Alves, I. (2022). Phytochemistry and biological activities of the floral hydroethanolic extract of *Ipomoea carnea* Jacq. (Convolvulaceae). Brazilian Journal of Science, 1(2), 1-7.

Mohanan, A., Nickerson, M. T., Ghosh, S. (2018). Oxidative stability of flaxseed oil: Effect of hydrophilic, hydrophobic and intermediate polarity antioxidants. *Food Chem*, *266*, 524–33. https://doi.org/10.1016/j.foodchem.2018.05.117.

Mora, A. S., Tayouo, R., Boutevin, B., David, G., Caillol, S. (2020). A perspective approach on the amine reactivity and the hydrogen bonds effect on epoxy-amine systems. *Eur Polym J*, *123*. https://doi.org/10.1016/j.eurpolymj.2019.109460.

Müller, C. M. O., Laurindo, J. B., Yamashita, F. (2011). Effect of nanoclay incorporation method on mechanical and water vapor barrier properties of starch-based films. *Ind Crops Prod*, *33*, 605–10. https://doi.org/10.1016/j.indcrop.2010.12.021.

Munteanu, S. B., Vasile, C. (2020). Vegetable additives in food packaging polymeric materials. *Polymers (Basel)*, *12*, 1-36. https://doi.org/10.3390/polym12010028.

Nandane, A. S., Jain, R. (2015). Study of mechanical properties of soy protein based edible film as affected by its composition and process parameters by using RSM. *J Food Sci Technol*, *52*, 3645-650. https://doi.org/10.1007/s13197-014-1417-4.

Ortega-Toro, R, Jiménez, A, Talens, P, Chiralt, A. (2014). Effect of the incorporation of surfactants on the physical properties of corn starch films. *Food Hydrocoll*, *38*, 66-75. https://doi.org/10.1016/j.foodhyd.2013.11.011.

Paglione, I. dos S., Galindo, M. V., de Souza, K. C., Yamashita, F., Grosso, C. R. F., Sakanaka, L. S., et al. (2019). Optimization of the conditions for producing soy protein isolate films. *Emirates J Food Agric*, *31*,

297–303. https://doi.org/10.9755/ejfa.2019.v31.i4.1933.

Peng, Y., Nair, S. S., Chen, H., Yan, N., Cao, J. (2018). Effects of Lignin Content on Mechanical and Thermal Properties of Polypropylene Composites Reinforced with Micro Particles of Spray Dried Cellulose Nanofibrils. *ACS Sustain Chem & Eng*, *6*, 11078–11086. https://doi.org/10.1021/acssuschemeng.8b02544.

Pradyawong, S., Qi, G., Li, N., Sun, X. S., Wang, D. (2017). Adhesion properties of soy protein adhesives enhanced by biomass lignin. *Int J Adhes Adhes*, *75*, 66-73. https://doi.org/10.1016/j.ijadhadh.2017.02.017.

Qin, Z., Mo, L., Liao, M., He, H., Sun, J. (2019). Preparation and characterization of soy protein isolate-based nanocomposite films with cellulose nanofibers and nano-silica via silane grafting. *Polymers (Basel)*, *11*. https://doi.org/10.3390/polym11111835.

Rajha, H. N., Abi-Khattar, A. M., El Kantar, S., Boussetta, N., Lebovka, N., Maroun, R. G., et al. (2019). Comparison of aqueous extraction efficiency and biological activities of polyphenols from pomegranate peels assisted by infrared, ultrasound, pulsed electric fields and high-voltage electrical discharges. *Innov Food Sci Emerg Technol*, *58*, 102212. https://doi.org/10.1016/j.ifset.2019.102212.

Ray, S., Cooney, R. P. (2018) Thermal degradation of polymer and polymer composites. *Handb. Environ. Degrad. Mater. Third Ed.*, 185–206. https://doi.org/10.1016/B978-0-323-52472-8.00009-5.

Rehman, A., Jafari, S. M., Aadil, R. M., Assadpour, E., Randhawa, M. A., Mahmood, S. (2020). Development of active food packaging via incorporation of biopolymeric nanocarriers containing essential oils. *Trends Food Sci Technol*, *101*, 106–21. https://doi.org/10.1016/j.tifs.2020.05.001.

Sattler, K. (2019). Advances in engineering research. *29*.

Siddaiah, T., Ojha, P., Kumar, N. O. G. V. R., Ramu, C. (2018). Structural, Optical and Thermal Characterizations of PVA/MAA:EA Polyblend Films. *Mater Res*, *21*. https://doi.org/10.1590/1980-5373-mr-2017-0987.

Siracusa, V. (2012). Food packaging permeability behaviour: A report. *Int J Polym Sci*, *2012*. https://doi.org/10.1155/2012/302029.

Su, L., Huang, J., Li, H., Pan, Y., Zhu, B., Zhao, Y., et al. (2021). Chitosan-riboflavin composite film based on photodynamic inactivation technology for antibacterial food packaging. *Int J Biol Macromol*, *172*, 231-240. https://doi.org/10.1016/j.ijbiomac.2021.01.056.

Tang, C. H., Chen, Z., Li, L., Yang, X. Q. (2006). Effects of transglutaminase treatment on the thermal properties of soy protein isolates. *Food Res Int*, *39*, 704-711. https://doi.org/10.1016/j.foodres.2006.01.012.

Tayeb, A. H., Tajvidi, M., Bousfield, D. (2020). Paper-based oil barrier packaging using lignin-containing cellulose nanofibrils. *Molecules*, *25*. https://doi.org/10.3390/molecules25061344.

Tylewicz, U., Oliveira, G., Alminger, M., Nohynek, L., Dalla Rosa, M., Romani, S. (2020). Antioxidant and antimicrobial properties of organic fruits subjected to PEF-assisted osmotic dehydration. *Innov Food Sci Emerg Technol*, *62*, 102341. https://doi.org/10.1016/j.ifset.2020.102341.

Vilas, C., Mauricio-Iglesias, M., García, M. R. (2020). Model-based design of smart active packaging systems with antimicrobial activity. *Food Packag Shelf Life*, *24*, 100446. https://doi.org/10.1016/j.fpsl.2019.100446.

Wang, C., Jiang, L., Wei, D., Li, Y., Sui, X., Wang, Z., et al. (2011). Effect of secondary structure determined by FTIR spectra on surface hydrophobicity of soybean protein isolate. *Procedia Eng*, *15*, 4819–4827. https://doi.org/10.1016/j.proeng.2011.08.900.

Wang, H., Hu, D., Ma, Q., Wang, L. (2016) Physical and antioxidant properties of flexible soy protein isolate films by incorporating chestnut (Castanea mollissima) bur extracts. *LWT - Food Sci Technol*, *71*, 33–39. https://doi.org/10.1016/j.lwt.2016.03.025.

Wang, H., Wang, L. (2017). Developing a bio-based packaging film from soya by-products incorporated with valonea tannin. *J Clean Prod, 143*, 624–33. https://doi.org/10.1016/j.jclepro.2016.12.064.

Wang, K., Amin, K., An, Z., Cai, Z., Chen, H., Chen, H., et al. (2020). Advanced functional polymer materials. *Mater Chem Front*, *4*, 1803-915. https://doi.org/10.1039/d0qm00025f.

Yan, Z., Li, Q., Zhang, P. (2017). Soy Protein Isolate and Glycerol Hydrogen Bonding Using Two-Dimensional Correlation (2D-COS) Attenuated Total Reflection Fourier Transform Infrared (ATR FT-IR) Spectroscopy. *Appl Spectrosc*, *71*, 2437–45. https://doi.org/10.1177/0003702817710249.

Zadeh, E. M., O'Keefe, S. F., Kim, Y. T. (2018). Utilization of Lignin in Biopolymeric Packaging Films. *ACS*

Omega, *3*7388–98. https://doi.org/10.1021/acsomega.7b01341.

Zhang, S., Xia, C., Dong, Y., Yan, Y., Li, J., Shi, S. Q., et al. (2016). Soy protein isolate-based films reinforced by surface modified cellulose nanocrystal. *Ind Crops Prod*, *80*, 207–13. https://doi.org/10.1016/j.indcrop.2015.11.070.

Zhong, Y., Godwin, P., Jin, Y., Xiao, H. (2020). Biodegradable polymers and green-based antimicrobial packaging materials: A mini-review. *Adv Ind Eng Polym Res, 3*, 27–35. https://doi.org/10.1016/j.aiepr.2019.11.002.

Zhu, J., Yan, C., Zhang, X., Yang, C., Jiang, M., Zhang, X. (2020). A sustainable platform of lignin: From bioresources to materials and their applications in rechargeable batteries and supercapacitors. *Prog Energy Combust Sci, 76*, 100788. https://doi.org/10.1016/j.pecs.2019.100788.

Copyrights